PCCP
Physical Chemistry Chemical Physics

Accepted Manuscript

This article can be cited before page numbers have been issued, to do this please use: M. Juanes, R. T. Saragi, R. Pinacho, J. E. Rubio and A. Lesarri, *Phys. Chem. Chem. Phys.*, 2020, DOI: 10.1039/D0CP01706J.

This is an Accepted Manuscript, which has been through the Royal Society of Chemistry peer review process and has been accepted for publication.

Accepted Manuscripts are published online shortly after acceptance, before technical editing, formatting and proof reading. Using this free service, authors can make their results available to the community, in citable form, before we publish the edited article. We will replace this Accepted Manuscript with the edited and formatted Advance Article as soon as it is available.

You can find more information about Accepted Manuscripts in the Information for Authors.

Please note that technical editing may introduce minor changes to the text and/or graphics, which may alter content. The journal's standard Terms & Conditions and the Ethical guidelines still apply. In no event shall the Royal Society of Chemistry be held responsible for any errors or omissions in this Accepted Manuscript or any consequences arising from the use of any information it contains.

ROYAL SOCIETY OF CHEMISTRY

rsc.li/pccp

View Article Online
DOI: 10.1039/D0CP01706J

Sulfur Hydrogen Bonding and Internal Dynamics in the Monohydrates of Thenyl Mercaptan and Thenyl Alcohol†

Marcos Juanes,[a] Rizalina Tama Saragi,[a] Ruth Pinacho,[b] José E. Rubio,[b] Alberto Lesarri,*[a]

[a]Departamento de Química Física y Química Inorgánica and I.U. CINQUIMA, Facultad de Ciencias, Universidad de Valladolid, Paseo de Belén, 7, 47011 Valladolid (Spain), E-mail: alberto.lesarri@uva.es, web: www.uva.es/lesarri

[b]Departamento de Electrónica, Escuela de Ingeniería de Telecomunicaciones, Universidad de Valladolid, Paseo de Belén, 15, 47011 Valladolid (Spain)

†Electronic Supplementary Information (ESI) available: Figures S1-S5 and Tables S1-S41 with computational predictions, rotational parameters for the monomers, experimental rotational transitions, rotational parameters for the minor isotopologues and structural calculations. See DOI: xx.xxxx/xxxxxxxxxx.

View Article Online
DOI: 10.1039/D0CP01706J

ABSTRACT

The monohydrates of thenyl alcohol and thenyl mercaptan have been probed in a supersonic jet expansion using chirped-pulsed and Fabry-Perot Fourier-transform microwave spectroscopy. The rotational spectra revealed a single isomer for each of the dimers. The thenyl alcohol hydrate is stabilized by an O-H···O_w hydrogen bond between the alcohol and water, with water acting as proton acceptor and additionally engaging in a O_w-H···π interaction with the thenyl ring. Conversely, water behaves as proton donor in the thenyl mercaptan hydrate, linking to the thiol group though a O_w-H···S hydrogen bond and secondary O_w-H···π interactions to the ring. In both dimers water retains internal mobility, as tunneling doublings in the spectrum confirm an internal rotation motion of water inside the cluster. The experimental results have been complemented with density-functional-theory molecular orbital calculations, binding energy decomposition and a topological analysis of the electronic density, providing a comparative description of the effects of hydrogen bonding of water to the alcohol and thiol groups in the dimers, relevant to understand hydrogen bonding to sulfur centers.

Keywords:

Non-covalent Interactions, Sulfur Hydrogen Bonding, Rotational Spectroscopy, Jet Spectroscopy, Microsolvation, Thenyl mercaptan, Thenyl alcohol

Introduction

Non-covalent interactions (NCI) involving sulfur centers are still undercharacterized,[1,2] despite recent theoretical and experimental investigations signalling a variety of chemical roles as σ and π H-bond donor (S-H···O, S-H···S, S-H···π, etc) and acceptor (O-H···S, N-H···S, etc),[3] the participation of σ/π holes of Group 16 atoms as electrophilic attractors in chalcogen bonds[4,5] and the influence of sulfur contacts in the functional properties of proteins and organic crystals.[6] In consequence, molecular studies are justified to contribute information on the structure, physical nature and balance of electrostatic and dispersive forces in NCI involving sulfur centers. In particular, the observation of weakly-bound intermolecular clusters in the gas phase simultaneously provides empirical data unbiased by crystal or matrix effects and validation of theoretical models. Vibrational evidence of sulfur hydrogen bonding generally originates from IR,[7] and double-resonance (UV–UV or IR–UV) laser spectroscopy,[1,2,8] but is mostly of low resolution and not always structurally univocal. High-resolution rotationally-resolved[9,10] studies are still scarce, as illustrated by the hydrogen sulphide dimer, reported only in 2018.[11] To date, rotational spectroscopy has addressed several intra-[12,13,14] and intermolecular interactions in hydrogen sulfide dimers or sulfur-containing complexes, like O-H···S,[15] F-H···S,[16] C-H···S,[17] S-H···S,[11] S-H···N[18] and S-H···π.[19,20,21] The gas-phase information can thus complement previous molecular descriptions relying solely on crystal data[3] and theoretical calculations.[1,22,23,24]

We recently observed in a jet expansion the H-bonds established by furfuryl mercaptan (FM) and its alcohol analogous (FA) in the monohydrates FM···H_2O and FA···H_2O (**1**, **2** in Scheme 1),[25] examining the differences between the oxygen and

View Article Online
DOI: 10.1039/D0CP01706J

sulfur interactions. Furfuryl alcohol forms a single insertion dimer with water, stabilized by two simultaneous H-bonds of dominant electrostatic character. In the primary interaction the alcohol acts as proton donor to water (O-H···O_w), while water donates a proton to the oxygen ring (O_w-H···O_r). Conversely, two isomers are observed when furfuryl mercaptan binds to water, the stronger interaction now being the water-to-ring (O_w-H···O_r) H-bond. In this case the thiol group may act both as H-bond donor (S-H···O_w) or acceptor (O_w-H···S) to water, forming a secondary H-bond. The mercaptan dimer is still dominantly electrostatic, but with a larger dispersion contribution. Would the further replacement of the ring oxygen by sulfur enhance the interaction between water and the thiol group? Moreover, could water establish two simultaneous hydrogen bonds with sulfur atoms as it does with oxygen in furfuryl alcohol? These questions are addressed in this comparative study of thenyl mercaptan (TM), thenyl alcohol (TA) and their monohydrates (TM···H_2O and TA···H_2O), which has confirmed a floppy interaction and a dynamic torsional behaviour of water in the two dimers (**3**, **4** in Scheme 1), quite different to the furfuryl hydrates.

Experimental and Computational Methods

Thenyl mercaptan (2-thiophenemethanethiol, >95% GC, b.p. 76°C) and thenyl alcohol (2-thiophenemethanol, >98% GC, b.p. 207°C) were obtained commercially and used without further purification. The vapors of each compound were diluted within a stream of pure neon (backing pressures of ca. 0.25 MPa), forming a supersonic jet by expansion through a pin-hole nozzle (ϕ=0.5-0.8 mm) into a high-vacuum chamber (ultimate pressures of 10^{-7} hPa). The mercaptan sample was volatile enough to be placed in an external reservoir inserted in the gas line, but the alcohol required a heating nozzle

(45°C) to obtain sufficient vapor pressure. For the water clusters either $H_2{}^{16}O$ or $H_2{}^{18}O$ were added to the gas line. The jet was probed with a broadband chirped-pulse Fourier transform microwave (CP-FTMW) spectrometer, operating in the region 2-8 GHz, and a Balle-Flygare cavity FTMW spectrometer, working in 8-18 GHz. The CP-FTMW spectrometer is based in a direct-digital design following Pate,[26] exciting the jet with a sequence of 5 short microwave chirped pulses (4 μs, 20 W) per molecular pulse. The pulsed jet had typical durations of 800-900 μs and propagated vertically, perpendicular to the emitting and receiving horn antennas. The detection of the transient emission resulting from rotational decoherence used a digital oscilloscope (20 MSamples/s), acquiring the time-domain signal for 40 μs per excitation pulse. The Fourier transformation with a Kaisser-Bessel window resulted in FWHM linewidths smaller than 150 kHz. For the present experiment 1 million averages were acquired at a repetition rate of 5 Hz. The uncertainty of the frequency measurements was estimated below 20 kHz. The cavity FTMW instrument excites the sample at a single frequency, using a coaxial arrangement of the jet and the microwave Fabry-Perot resonator.[27] The resonator reduces the power excitation requirements (1 μs, 100 mW), simultaneously producing longer interaction times with the radiation. The time-domain signal is acquired over 400 μs, resulting in better resolution (FWHM linewidths below 15 kHz). However, the cavity operation bandwidth is limited to ca. 1 MHz, requiring a mechanical retuning for frequency scanning. Additionally, the coaxial arrangement splits the resonance frequency into two Doppler components. Frequency uncertainties are estimated below 5 kHz.

The experimental study was complemented with computational calculations. Following an initial conformational screening with molecular mechanics (MMFF[28]), all further calculations used density-functional theory (DFT) molecular orbital calculations.

Two density-functional methods were tested here, including the well-known B3LYP[29] hybrid and Truhlar's meta-GGA MN15-L[30] functional, in combination with Ahlrichs' polarized triple-zeta basis def2-TZVP.[31] The Minnesota functional was assumed parametrized for dispersion. B3LYP was supplemented with D3[32] dispersion corrections and Becke-Johnson damping.[33] For the two most stable conformers of the monohydrates additional B2PLYP-D3(BJ)[34] and ωB97XD[35] were later conducted with the same basis set. Electronic energies were supplemented with zero-point energy corrections. Frequency calculations were performed at the same level of theory, using the harmonic approximation. The calculation of interaction energies considered the basis set superposition errors (BSSE) with the counterpoise approximation,[36] and refers to the monomers in the configuration of the complex. All DFT calculations were conducted with Gaussian 16,[37] using default convergence criteria and a "ultrafine" grid for numerical integration. The physical contributions to the binding potential of the water clusters were estimated by energy decomposition analysis using zeroth-order symmetry adapted perturbation theory[36,38] (SAPT), implemented in PSI4.[39] Finally, the presence of non-covalent interactions was analyzed with the NCIPlot methodology, based on a reduced gradient of the electronic density[40,41]

Results and Discussion

1. TM and TA monomers

The experimental work initially examined the conformational landscape and rotational spectrum of the thenyl monomers TM and TA, previously unreported. Similarly to the furfuryl derivatives,[25] the bidimensional potential energy surface is defined by two dihedrals describing the elevation of the side chain with respect to the thenyl ring

View Article Online
DOI: 10.1039/D0CP01706J

(τ_1(S1-C2-C6-S7/O7) and the orientation of the terminal thiol/alcohol hydrogen atom (τ_2(C2-C6-S7/O7-H). Molecular orbital calculations in Tables S1-S2 (ESI†) predicted elevation angles close to +60° (τ_1 +gauche or G) for the side chain (as in the furfuryl derivatives) and staggered orientations for the terminal alcohol/thiol. However, the terminal hydrogen atom now preferentially orients to the adjacent carbon-carbon bond in the ring π system (τ_2 +gauche or G) of TM or TA instead of pointing to the ring oxygen as in FA or FM, inverting the conformational stability of the furfuryl compounds. DFT energetic predictions in Tables S3-S4 and Figures S1-S2 (ESI†) suggest that the second GG´ conformation is 1.2-1.9 kJ mol^{-1} above the global minimum GG at B3LYP-D3(BJ) level.

The jet-cooled microwave spectra of water-seeded TM and TA is shown in Figures 1 and 2. Following the initial predictions the rotational spectra of the two monomers were readily assigned based on their dominant μ_a and μ_b selection rule transitions. A smaller set of weaker μ_c transitions were added later. The spectrum was analysed using a conventional Watson's (S-reduced) semirigid-rotor Hamiltonian[42] including up to quartic terms in the centrifugal distortion, implemented with Pickett's SPFIT program.[43] In the two molecules the spectral intensity was sufficient to assign independently the parent and all monosubstituted ^{13}C and ^{34}S isotopologues in natural abundance (1% and 4%, respectively). The resulting rotational parameters for TM and TA are collected in Tables S5 and S6, while the present dataset of measured transitions are collected in Tables S7-S14 (TM) and S15-S21 (TA), ESI†. A structural analysis using effective and substitution methods[44] in Tables S22-S27 (ESI†) was consistent with the detection of the predicted global minimum GG for the two thenyl monomers. The structural calculations used Rudolph's MOMSTRUC programs.[45]

View Article Online
DOI: 10.1039/D0CP01706J

2. TA and TM monohydrates

The investigation of the TM and TA monohydrates started from the computational molecular models in Tables 1-2. For TA···H_2O five isomers were found with Gibbs energy below 8 kJ mol^{-1}. As expected, the microsolvation of the alcohol always involves a primary H-bond between the water molecule and the hydroxyl group in the side chain, as shown in Figure 3 (isomer notation indicates the GG/GG´/AG´ monomer conformation and the water donor/acceptor role). Conversely, attractive contacts with the thenyl sulfur atom are avoided, so water forms addition complexes either on top or laterally to the ring, which occasionally allows a secondary interaction with the π ring system. While water may act both as proton donor or acceptor to the alcohol the predictions suggest a marked preference for the alcohol to behave as proton donor to water, with other isomers well separated in energy (B3LYP-D3(BJ): 4-5 kJ mol^{-1}, MN15-L: 1-8 kJ mol^{-1}). The conformational options for the mercaptan monohydrate TM···H_2O in Figure 4 are less clearly defined. According to B3LYP-D3(BJ) four isomers are very close in energy (< 1.8 kJ mol^{-1}), while the fifth isomer is located at 3.4 kJ mol^{-1}. Using MN15-L two isomers are practically isoenergetic (0.9 kJ mol^{-1}) and the rest have conformational energies of 2.7-5.2 kJ mol^{-1}. In both cases the global minimum corresponds to the thiol group acting as proton donor to water, establishing a primary S-H···O_w hydrogen bond, which is accompanied by water interactions to the ring. In all isomers there are no direct interactions between water and the thenyl sulfur atom, except in the less stable isomer, where water simultaneously links to this atom and the π electronic cloud.

The close conformational energies demanded an experimental verification of the computational models. The microwave spectrum of TA···H_2O in Figure 1 was first analysed, using the predicted rotational constants of Table 1. A single isomer was then

assigned, characterized by a set of both R- (J+1←J) and Q-branch (J←J) μ_b and additional R-branch μ_a rotational transitions, spanning quantum numbers J=0-7 and K_{-1}<3. The most relevant spectral feature was a small (0.1-0.6 MHz) tunnelling doubling in both μ_a and μ_b transitions, confirming a large-amplitude internal motion connecting two symmetry-equivalent structures. The relative intensities of the two tunnelling components was close to 3:1, coincident with the nuclear spin statistical weights associated to the exchange of two fermions with spin I=1/2. In consequence, the spectral doublings confirm an internal rotation of water around its symmetry axes in the cluster, splitting the ground vibrational state in two torsional sublevels 0^- and 0^+. The observed splittings correspond to intra-state $0^{\pm} \leftrightarrow 0^{\pm}$ torsional-rotational transitions, with inter-state transitions $0^{\mp} \leftrightarrow 0^{\pm}$ forbidden. The rovibrational analysis used a two-state Hamiltonian $\boldsymbol{H}_{RV}$ comprising rigid ($\boldsymbol{H}_{0^+}^{R}$, $\boldsymbol{H}_{0^-}^{R}$) and semirigid-rotor ($\boldsymbol{H}_{0^+}^{CD}$, $\boldsymbol{H}_{0^-}^{CD}$) Watson terms[42] for both states, the energy separation ($\Delta E_{0^{\pm}}$) and plausible interaction terms ($\boldsymbol{H}_{int}$) according to

$$\boldsymbol{H}_{RV} = \begin{pmatrix} \boldsymbol{H}_{0^-}^{R} + \boldsymbol{H}_{0^-}^{CD} & \boldsymbol{H}_{int} \\ \boldsymbol{H}_{int} & \boldsymbol{H}_{0^+}^{R} + \boldsymbol{H}_{0^+}^{CD} + \Delta E_{0^{\pm}} \end{pmatrix} \quad (1)$$

However, neither the interaction terms or the energy separation were determinable from our experimental dataset, which effectively behaved like two independent rotors. The final spectroscopic results are collected in Table 3. Because of the good intensity of the cluster the ^{34}S-thenyl isotopologue was additionally measured in natural abundance. The investigation proceeded also to the ^{18}O-water cluster, unequivocally confirming the assignment. The rotational parameters of ^{34}S-TA···$H_2{}^{16}$O and TA···$H_2{}^{18}$O are shown in Tables S28-S29 (ESI†), while all the measured transitions are collected in Tables S30-S32 (ESI†).

The study of the thenyl mercaptan monohydrate TM···H_2O was based in the microwave spectrum in Figure 2, which revealed a single isomer with only R-branch μ_a transitions and quantum numbers in the range J=1-9 and K_{-1}<5. Small tunnelling splittings of 0.2-0.4 MHz with relative intensities close to 3:1 were also apparent, similarly leading to the conclusion that water is engaging internally in internal rotation around its axis, symmetrically inverting two half spin fermions. A fit of the rotational transitions to the two-state Hamiltonian of eqn. (1) did not show noticeable couplings, and the two torsional states again behaved as independent rotors. The assignment was confirmed by observation of the ^{18}O-water dimer TM···$H_2{}^{18}O$. The derived rotational parameters are found in Table 4 and Table S33 (ESI†), with the full listing of transitions in Tables S34-S35 (ESI†).

3. Molecular structures of the monohydrates

The structural analysis of the monohydrates of thenyl alcohol and thenyl mercaptan used the effective (r_0) and substitution methods (r_s), described elsewhere.[46] In both cases the rotational constants, the substitution coordinates of the water oxygen atom and the derived effective structures give an unambiguous identification of the thenyl-water dimers. In the thenyl alcohol hydrate the conformational assignment immediately pointed to the predicted global minimum GG-Wa in Figures 3 and S3 (ESI†), as observed by comparison between the experimental and predicted rotational constants in Tables 1 and 3. In this dimer the B3LYP-D3(BJ) predictions performed much better than MN15-L (relative deviations of 0.4-1.4% compared to 3.6-7.4%, respectively). Comparative B2PLYP and ωB97XD predictions are given in Table S36 (ESI†). This assignment is consistent with the substitution coordinates of the thenyl sulfur and water oxygen atoms in Table S37 (ESI†). An effective structure for TA···H2O was derived by

View Article Online
DOI: 10.1039/D0CP01706J

fitting three molecular parameters: the $r(H\cdots O_w)$ distance between the water oxygen and the bridging hydrogen atom, the $\angle(O\text{-}H\cdots O_w)$ linearity angle between the alcohol group and the water oxygen and the $\tau(C\text{-}O\text{-}H\cdots O_w)$ dihedral angle between the alcohol side chain and the water oxygen. The resulting fit in Table S38 (ESI†) reproduces the nine rotational constants below 1 MHz, with a root-mean-square (rms) residual of 0.4 MHz. Non-fitted parameters were constrained to the B3LYP-D3(BJ) structure in Table S39 (ESI†).

The identification of the thenyl mercaptan hydrate was more difficult, as more isomers are expected within a small energy range. However, the comparison of the rotational constants in Tables 2 and 4 clearly points to the second isomer GG´-Wdπ of Figures 4 and S4 (ESI†), identified as second most stable structure. The predicted global minimum, which was actually similar to that of $TA\cdots H_2O$, was not observed, reflecting deficiencies of the DFT energetic calculations to identify the lowest-lying geometry for the weaker sulfur interaction. B3LYP-D3(BJ) and MN-15L predict the second isomer at 1.3-2.7 kJ mol^{-1} above the global minimum, which may be within the calculation uncertainty. Additional B2PLYP-D3(BJ) and B97XD in Table S40 (ESI†) suggest relative energies of 2.5-2.7 kJ mol^{-1}. No other low-energy isomers were observed. The absence of additional isomers for $TA\cdots H_2O$ and $TA\cdots H_2O$ cannot be attributed to thermodynamic stability alone, as populations in jet experiments are affected by the pathways and energy barriers involved in conformational interconversion, making collisional relaxation a significant kinetic factor.[47]

Structurally, the prediction of rotational constants showed again better accuracy for the B3LYP-D3(BJ) method (0.2-1.3% vs 0.2-3.2 for MN15-L). The identification of isomer GG´-Wdπ was confirmed by the water oxygen substitution coordinates of Table S41 (ESI†) and the effective structure of Table S42 (ESI†). For $TM\cdots H_2O$ the structural

fit included the $r(H_w\cdots S)$ distance between the water hydrogen to the thiol sulfur atom, the $\angle(C\text{-}S\cdots H_w)$ orientation angle of the bridging hydrogen and the $\tau(C\text{-}C\text{-}S\cdots H_w)$ dihedral, all other parameters fixed to the B3LYP-D3(BJ) coordinates of Table S43 (ESI†). Because only two isotopologues were available for $TM\cdots H_2O$ the effective structure gives a worse reproduction of the experimental rotational constants (deviations <2.2 MHz, rms residual of 1.1 MHz) compared to $TA\cdots H_2O$.

4. Non-covalent interactions

The non-covalent interactions in $TA\cdots H_2O$ and $TM\cdots H_2O$ have been analysed structurally, energetically and using the electronic density topology. For comparison purposes Figure 5 shows the monohydrates of the two thenyl and the two furfuryl compounds of ref. 25. From a structural point of view thenyl alcohol forms a $O\text{-}H\cdots O_w$ H-bond to water, which behaves as proton acceptor (r_0: $r(H\cdots O_w)$=1.984(4) Å, B3LYP-D3(BJ): 1.965 Å). This situation is similar to furfuryl alcohol (r_0: $r(H\cdots O_w)$=1.956(3), B3LYP-D3(BJ): 1.925 Å). However, while in the furfuryl compounds water may bind secondarily to the ring oxygen, the interaction of water with the thenyl compounds avoids the ring sulfur atom and gives priority to the interaction with the π electronic cloud through $O_w\text{-}H\cdots\pi$ interactions. In thenyl mercaptan there is no leading hydroxyl interaction and water is forced to behave as proton donor to the thiol group though a long $O\text{-}H\cdots S$ H-bond (r_0: $r(H\cdots O_w)$= 2.634(18) Å, B3LYP-D3(BJ): 2.579 Å). The situation is reminiscent of the primary interaction in the furfuryl mercaptan - water cluster, where $O\text{-}H\cdots S$ and $S\text{-}H\cdots O$ H-bonds both were detected. Interestingly, the conformation of thenyl alcohol in the monohydrate retains the most stable conformation of the monomer (GG), while in the thenyl mercaptan hydrate the monomer changes its conformation to the higher-energy structure GG´ to accommodate the $O\text{-}H\cdots S$ H-bond.

View Article Online
DOI: 10.1039/D0CP01706J

This fact is consistent with collisionally affordable barriers for the GG↔GG' interconversion (Figure S1, ESI†). Conformational changes induced by molecular aggregation have been occasionally reported.[48,49]

From the energetic point of view two aspects are noticeable. The (B3LYP-D3(BJ)) complexation energies in Tables 1-2 and Ref. 25 (relative to the monomer conformations in the complexes) are ca. 9-12 kJ mol^{-1} weaker in the thenyl compounds than in the furfuryl equivalents, following the trend: FA···H_2O (-35.0 kJ mol^{-1}) < TA···H_2O (-33.2 kJ mol^{-1}) < TM···H_2O (-24.1 kJ mol^{-1}) ~ FM···H_2O (-23.8 kJ mol^{-1}). In consequence, the absence of the alcohol group considerably decreases the magnitude of the intermolecular interactions in the dimer, reflecting the weaker H-bonds established by sulfur. Experimental binding energies for the O-H···S H-bond have been determined only for phenol···H_2S and fluorophenol···H_2S, using ZEKE photoelectron spectroscopy.[50,51] The experimental ground-state value of D_0 = -13.2(4) kJ mol^{-1} in phenol···H_2S is ca. 6% lower than our B3LYP-D3(BJ) calculations for this cluster (D_0 = -14.1 kJ mol^{-1}, D_e = -18.8 kJ mol^{-1}), suggesting that the computational complexation energies for the mercaptans may be larger by a similar factor. A second point concerns the contribution of dispersive interactions. All four furfuryl and thenyl monohydrates are dominantly electrostatic, as observed in Table 5 from a binding energy decomposition using SAPT(0)/jun-cc-pVDZ.[36,38] However, there is a considerable increase in the dispersion contribution when passing from the theny alcohol to the thenyl mercaptan hydrates, moving from 55.4% to 83.3% of the total binding energy. This increment was less notorious in the hydrates of furfuryl alcohol (43.6%) and furfuryl mercaptan (57.3-60.6%),[25] which both retain a O-H···O H-bond, absent in thenyl mercaptan. This calculation confirms the weaker and more dispersive character of the sulfur interactions in these molecules,[1,2,8,45] also observed in Table 5 for the

dimers of water[52] and hydrogen sulphide.[11] A calculation on the dominantly dispersive pyridine-methane[53] dimer is given also for comparison.

Non-covalent interactions have been analyzed also using NCIPlot electronic density mapping.[40,41] This method evaluates a reduced electronic density gradient s $\left(=\frac{1}{1(3\pi^2)^{1/3}\rho^{4/3}}\right)$ versus a signed electronic density $(\mathrm{sign}\,(\lambda_2)\,\rho)$ using the second eigenvalue (λ_2) of the electron density Hessian (Figure S5, ESI†). The NCIPlots in Figure 5 compare the four furfuryl and thenyl hydrates, revealing well-defined O-H···O H-bond regions (associated to bond critical points), together with weaker interactions associated to the O-H···S H-bond and, finally, broad surfaces of weak interactions between the water molecule and the π ring, most notorious in thenyl mercaptan. The NCIPlot analysis thus confirms the presence of multiple interactions in the hydrates and the gradation of attractive interactions on passing from oxygen to sulfur in these five-membered ring molecules.

Conclusion

The combination of jet-cooled (chirped-pulsed) broadband rotational spectroscopy,[9] molecular orbital calculations,[29,33] binding energy decomposition[36,38] and electronic density topological analysis[40] provided a comprehensive description of the non-covalent interactions in the monohydrates of thenyl alcohol and thenyl mercaptan, simultaneously emphasizing the role of gas-phase intermolecular clusters as functional and size-specific models of molecular aggregation.

The molecular data on the two thenyl hydrates and the previous analysis of furfuryl alcohol and furfuryl mercaptan[25] allowed a comparative study in which the oxygen atoms were successively replaced by one or two sulfur atoms, offering quantitative information on the decrease in binding energy, increment of the role of

dispersion interactions and structural rearrangement associated to the loss of the strong O-H···O hydroxyl to water H-bond. In addition, the presence of a thenyl group instead of the furfuryl ring prevented the interactions of water to the ring heteroatom, resulting in a floppy character of the two thenyl hydrates, where water retains the capacity to engage in large-amplitude internal motions, as revealed by the torsional tunneling splittings in the rotational spectra. The nature of hydrogen bonding to sulfur centers and other low-electronegativity atoms,[1-3] together with the correlation between weaker interactions and increased isomerism and intramolecular large-amplitude motions[54] remains a topic still under-investigated, calling for additional high-resolution molecular studies.

Finally, the importance of accurate DFT dispersion models for the description of weakly-bound complexes should be emphasized. As illustration, the worse behavior of the MN15-L functional in the present study may suggest the need to introduce explicit long-range dispersion corrections in the Minnesota functionals.[55] This fact illustrates the contribution and complementary role of empirical data from high-resolution rotational data for the development of DFT computational models of molecular aggregation.

Acknowledgements

Funding from the Spanish MICINN-FEDER (PGC2018-098561-B-C22) and JCyL (grant VA056G18) is gratefully acknowledged. M.J. and R. T. S. thank predoctoral contracts from the MICINN and UVa, respectively.

DOI: 10.1039/D0CP01706J

References

1 H. S. Biswal, Hydrogen Bonding Involving Sulfur: New Insights from Ab Initio Calculations and Gas Phase Laser Spectroscopy, in *Noncovalent Forces* (Ed.: S. Scheiner), Chap. 2, Springer Int. Pub., Switzerland, 2015.

2 H. S. Biswal, S. Bhattacharyya, A. Bhattacherjee, S. Wategaonkar, Nature and Strength of Sulfur-Centred Hydrogen Bonds: Laser Spectroscopic Investigations in the Gas Phase and Quantum-chemical Calculations, *Int. Rev. Phys. Chem*., 2015, **34**, 99-160.

3 G. Gilli, P. Gilli, The Nature of the Hydrogen Bond, IUC-Oxford University Press, Oxford, 2009.

4 C. B. Aakeroy, D. L. Bryce, G. Desiraju, A. Frontera, A. C. Legon, F. Nicotra, K. Rissanen, S. Scheiner, G. Terraneo, P. Metrangolo, G. Resnati, Definition of the Chalcogen Bond, *Pure Appl. Chem*., 2019, **91**, 1889–1892.

5 a) I. Alkorta, J. Elguero, A. Frontera, Not Only Hydrogen Bonds: Other Noncovalent Interactions, *Crystals*, 2020, **10**, 180; b) A. C. Legon, Tetrel, Pnictogen and Chalcogen Bonds Identified in the Gas Phase Before they Had Names: a Systematic Look at Non-covalent Interactions, *Phys. Chem. Chem. Phys*., 2017, **19**, 14884–14896.

6 a) P. Zhou, F. Tian, F. Lv, Z. Shang, *Proteins*, Geometric Characteristics of Hydrogen Bonds Involving Sulfur Atoms in Proteins, 2009, **76**, 151–163. b) V. R. Mundlapati, S. Ghosh, A. Bhattacherjee, P. Tiwari, H. S. Biswal, Critical Assessment of the Strength of Hydrogen Bonds Between the Sulfur Atom of Methionine/Cysteine and Backbone Amides in Proteins, *J. Phys. Chem. Lett*., 2015, **6**, 1385–1389.

7 a) J. R. Goebel, B. S. Ault, J. E. Del Bene, Matrix Isolation and ab Initio Study of 1:1 Hydrogen-Bonded Complexes of H_2O_2 with Phosphorus and Sulfur Bases, *J. Phys. Chem. A*, 2001, **105**, 11365-11370; b) M. Wierzejewska, Infrared Matrix Isolation Studies of Complexes Formed Between Dimethylsulfide, Dimethyldisulfide and Nitrous Acid, *J. Mol. Struct*., 2000, **520**, 199–214.

8 a) D. Wang, P. Chopra, S. Wategaonkar, A. Fujii, Electronic and Infrared Spectroscopy of Benzene-$(H_2S)_n$ (n = 1 and 2): The Prototype of the SH-π Interaction, *J. Phys. Chem. A*, 2019, **123**, 7255-7260. b) S. Wategaonkar, A. Bhattacherjee, N-H···S Interaction Continues to Be an Enigma: Experimental and Computational Investigations

View Article Online
DOI: 10.1039/D0CP01706J

of Hydrogen-Bonded Complexes of Benzimidazole with Thioethers, *J. Phys. Chem. A*, 2018, **122**, 4313–4321. c) A. Bhattacherjee, Y. Matsuda, A. Fuji, S. Wategaonkar, The Intermolecular S–H···Y (Y=S, O) Hydrogen Bond in the H_2S Dimer and the H_2S–MeOH Complex, *ChemPhysChem*, 2013, **14**, 905–914; d) H. S. Biswal, S. Wategaonkar, OH···X (X = O, S) Hydrogen Bonding in Tetrahydrofuran and Tetrahydrothiophene, *J. Chem. Phys*., 2011, **135**, 134306.

9 W. Caminati, J.-U. Grabow, Advancements in Microwave Spectroscopy, Frontiers and Advances in Molecular Spectroscopy, Chapter 17, pp. 569–598, Elsevier, Amsterdam, 2018.

10 M. Juanes, R. T. Saragi, W. Caminati, A. Lesarri, The Hydrogen Bond and Beyond: Perspectives for Rotational Investigations of Non-covalent Interactions, *Chem. Eur. J*., 2019, **25**, 11402–11411.

11 A. Das, P. K. Mandal, F. J. Lovas, C. Medcraft, N. R. Walker, E. Arunan, The H_2S Dimer is Hydrogen-Bonded: Direct Confirmation from Microwave Spectroscopy. *Angew. Chem. Int. Ed*., 2018, **57**, 15199–15203.

12 L. H. Xu, Q. Liu, R. D. Suenram, F. J. Lovas, A. R. H. Walker, J. O. Jensen, A. C. Samuels, Rotational Spectra, Conformational Structures, and Dipole Moments of Thiodiglycol by Jet-cooled FTMW and Ab Initio Calculations, *J. Mol. Spectrosc*., 2004, **228**, 243–250.

13 G. C. Cole, H. Møllendal, J.-C. Guillemin, Microwave Spectrum of 3-Butyne-1-thiol: Evidence for Intramolecular S-H···π Hydrogen Bonding, *J. Phys. Chem. A*, 2006, **110**, 9370–9376.

14 M. Juanes, R. T. Saragi, Y. Jin, O. Zingsheim, S. Schlemmer, A. Lesarri, Rotational Spectrum and Intramolecular Hydrogen Bonding in 1,2-Butanedithiol *J. Mol Struct*., 2020, **1211**, 128080.

15 M. E. Sanz, J. C. López, J. L. Alonso, A. Maris, P. G. Favero, W. Caminati, Conformation and Stability of Adducts of Sulfurated Cyclic Compounds with Water: Rotational Spectrum of Tetrahydrothiophene−Water, *J. Phys. Chem. A*, 1999, **103**, 5285–5290.

View Article Online
DOI: 10.1039/D0CP01706J

16 S. A. Cooke, G. K. Corlett, A. C. Legon, Comparisons of the Interactions of Benzene, Furan and Thiophene with Lewis Acids: The Rotational Spectrum of Thiophene···HF, *Chem. Phys. Lett*., 1998, **291**, 269–276.

17 E. J. Cocinero, R. Sánchez, S. Blanco, A. Lesarri, J. C. López, J. L. Alonso, Weak Hydrogen Bonds C–H···S and C–H···F–C in the Thiirane–Trifluoromethane Dimer, *Chem. Phys. Lett*., 2005, **402**, 4–10.

18 M. J. Tubergen, J. E. Flad, J. E. del Bene, Microwave Spectroscopic and Ab Initio Studies of the Hydrogen-Bonded Trimethylamine–Hydrogen Sulfide Complex, *J. Chem. Phys*., 1997, **107**, 2227.

19 E. Arunan, T. Emilsson, H. S. Gutowski, G. T. Fraser, G. de Oliveira, C. E. Dykstra, Rotational Spectrum of the Weakly Bonded C_6H_6–H_2S Dimer and Comparisons to C_6H_6–H_2O Dimer *J. Chem. Phys*., 2002, **117**, 9766.

20 M. Goswami, E. Arunan, Microwave Spectrum and Structure of C_6H_5CCH···H_2S Complex, *J. Mol. Spectrosc*. 2011, **268**, 147–156.

21 M. Goswami, J. L. Neill, M. Muckle, B. H. Pate, E. Arunan, Microwave, Infrared-Microwave Double Resonance, and Theoretical Studies of C_2H_4···H_2S complex, *J. Chem. Phys*., 2013, **139**, 104303.

22 a) D. L. Crittenden, A Systematic CCSD(T) Study of Long-Range and Noncovalent Interactions between Benzene and a Series of First- and Second-Row Hydrides and Rare Gas Atoms, *J. Phys. Chem. A*, 2009, **113**, 1663-1669; b) A. Vila, R. A. Mosquera, Are the hydrogen bonds involving sulfur bases inverse or anomalous?, *Int. J. Quantum Chem.*, 2006, **106**, 928-934; c) T. P. Tauer, M. E. Derrick, C. D. Sherrill, Estimates of the Ab Initio Limit for Sulfur−π Interactions: The H_2S−Benzene Dimer, *J. Phys. Chem. A*, 2005, **109**, 191–196.

23 F. Wennmohs, V. Staemmler, M. Schindler, Theoretical Investigation of Weak Hydrogen Bonds to Sulfur, *J. Chem. Phys*., 2003, **119**, 3208–3218.

24 D. Kaur, D. Aulakh, S. Khanna, H. Singh, Theoretical Study on the Nature of S···H and O ··· H Hydrogen Bonds, *J. Sulfur Chem*., 2014, **35**, 290–303.

25 M. Juanes, A. Lesarri, R. Pinacho, E. Charro, J. E. Rubio, L. Enríquez, M. Jaraíz, Sulfur Hydrogen Bonding in Isolated Monohydrates: Furfuryl Mercaptan versus Furfuryl Alcohol, *Chem. Eur. J*., 2018, **24**, 6564–6571.

View Article Online
DOI: 10.1039/D0CP01706J

26 J. L. Neill, S. T. Shipman, L. Alvarez-Valtierra, A. Lesarri, Z. Kisiel, B. H. Pate, Rotational Spectroscopy of Iodobenzene and Iodobenzene–Neon with a Direct Digital 2–8 GHz Chirped-Pulse Fourier Transform Microwave Spectrometer, *J. Mol. Spectrosc*., 2011, **269**, 21–29.

27 J.-U. Grabow, W. Stahl, H. Dreizler, A multioctave coaxially oriented beam-resonator arrangement Fourier-transform microwave spectrometer, *Rev. Sci. Instrum.*, 1996, **67**, 4072–4084.

28 (a) M. Saunders, K. N. Houk, Y.-D. Wu, W. C. Still, M. Lipton, G. Chang, W. C. Guida, Conformations of Cycloheptadecane. A Comparison of Methods for Conformational Searching, *J. Am. Chem. Soc*., 1990, **112**, 1419–1427. (b) G. M. Keresu, I. Kolossváry, Fully Flexible Low-Mode Docking: Application to Induced Fit in HIV Integrase, *J. Am. Chem. Soc*., 2001, **123**, 12708–12709.

29 Becke, A. D. Density-Functional Thermochemistry. III. The Role of Exact Exchange. *J. Chem. Phys.*, 1993, **98**, 5648–5652.

30 Yu, H. S.; He, X.; Truhlar, D. G. MN15-L: A New Local Exchange-Correlation Functional for Kohn–Sham Density Functional Theory with Broad Accuracy for Atoms, Molecules, and Solids. *J. Chem. Theory Comput*., 2016, **12**, 1280–1293.

31 Weigend, F.; Ahlrichs, R. Balanced Basis Sets of Split Valence, Triple Zeta Valence and Quadruple Zeta Valence Quality for H to Rn: Design and Assessment of Accuracy, *Phys. Chem. Chem. Phys*., 2005, **7**, 3297–3305.

32 S. Grimme, S. Ehrlich, L. Goerigk, Effect of the Damping Function in Dispersion Corrected Density Functional Theory. *J. Comput. Chem*., 2011, **32**, 1456–1465

33 E. R. Johnson, A. D. Becke, A Post-Hartree-Fock Model of Intermolecular Interactions: Inclusion of Higher-order Corrections, *J. Chem. Phys.*, 2006, **124**, 174104.

34 S. Grimme, F. Neese, Double-hybrid density functional theory for excited electronic states of molecules, *J Chem Phys*. 2007, **127**,154116.

35 J.-D. Chai, M. Head-Gordon, Long-range Corrected Hybrid Density Functionals with Damped Atom-Atom Dispersion Corrections, *Phys. Chem. Chem. Phys*., 2008, **10**, 6615-6620.

36 S. Scheiner, Hydrogen Bond, A Theoretical Perspective, *Oxford University Press: Oxford*, 1997, and references therein.

View Article Online
DOI: 10.1039/D0CP01706J

37 Gaussian 16, Revision C.01, M. J. Frisch, G. W. Trucks, H. B. Schlegel, G. E. Scuseria, M. A. Robb, J. R. Cheeseman, G. Scalmani, V. Barone, G. A. Petersson, H. Nakatsuji, X. Li, M. Caricato, A. V. Marenich, J. Bloino, B. G. Janesko, R. Gomperts, B. Mennucci, H. P. Hratchian, J. V. Ortiz, A. F. Izmaylov, J. L. Sonnenberg, D. Williams-Young, F. Ding, F. Lipparini, F. Egidi, J. Goings, B. Peng, A. Petrone, T. Henderson, D. Ranasinghe, V. G. Zakrzewski, J. Gao, N. Rega, G. Zheng, W. Liang, M. Hada, M. Ehara, K. Toyota, R. Fukuda, J. Hasegawa, M. Ishida, T. Nakajima, Y. Honda, O. Kitao, H. Nakai, T. Vreven, K. Throssell, J. A. Montgomery, Jr., J. E. Peralta, F. Ogliaro, M. J. Bearpark, J. J. Heyd, E. N. Brothers, K. N. Kudin, V. N. Staroverov, T. A. Keith, R. Kobayashi, J. Normand, K. Raghavachari, A. P. Rendell, J. C. Burant, S. S. Iyengar, J. Tomasi, M. Cossi, J. M. Millam, M. Klene, C. Adamo, R. Cammi, J. W. Ochterski, R. L. Martin, K. Morokuma, O. Farkas, J. B. Foresman and D. J. Fox, *Gaussian, Inc., Wallingford CT*, 2016.

38 B. Jeziorski, R. Moszynski and K. Szalewicz, Perturbation Theory Approach to Intermolecular Potential Energy Surfaces of van der Waals Complexes, *Chem. Rev*., 1994, **94**, 1887–1930.

39 J. M. Turney, A. C. Simmonett, R. M. Parrish, E. G. Hohenstein, F. A. Evangelista, J. T. Fermann, B. J. Mintz, L. A. Burns, J. J. Wilke, M. L. Abrams, N. J. Russ, M. L. Leininger, C. L. Janssen, E. T. Seidl, W. D. Allen, H. F. Schaefer, R. A. King, E. F. Valeev, C. D. Sherrill and T. D. Crawford, PSI4: An Open-Source Ab Initio Electronic Structure Program, *Wiley Interdiscip. Rev.: Comput. Mol. Sci.,* 2012, **2**, 556–565.

40 J. Contreras-García, E. R. Johnson, S. Keinan, R. Chaudret, J.-P. Piquemal, D. N. Beratan, W. Yang, NCIPLOT: a Program for Plotting Noncovalent Interaction Regions, *J. Chem. Theor. Comput.*, 2011, **7**, 625–632.

41 J. R. Lane, J. Contreras-García, J.-P. Piquemal, B. J. Miller, H. G. Kjaergaard, Are Bond Critical Points Really Critical for Hydrogen Bonding?, *J. Chem. Theor. Comput*., 2013, **9**, 3263–3266.

42 J. K. G. Watson, in Vibrational Spectra and Structure, 6 (Ed.: J. R. Durig), Elsevier, Amsterdam, 1977, pp. 1–89.

43 H. M. Pickett, The Fitting and Prediction of Vibration-Rotation Spectra with Spin Interactions, *J. Mol. Spectrosc*. 1991, **148**, 371–377.

View Article Online
DOI: 10.1039/D0CP01706J

44 H. D. Rudolph, J. Demaison in Equilibrium Molecular Structures (Ed.: J. Demaison, J. E. Boggs, A. G. Császar), Chap. 5, pp. 125-158, CRC Press: Boca Raton, FL, 2011

45 MOMSTRUC Structural Package. Available at: https://www.uni-ulm.de/~hrudolph/ (last accessed: March 2020)

46 H. D. Rudolph, J. Demaison, in Equilibrium Molecular Structures: from Spectroscopy to Quantum Chemistry (J. Demaison, J. E. Boggs, A. G. Csaszar, Eds.), chap.5, pp. 125-158, CRC Press, Boca Ratón, FL, 2011

47 P. D. Godfrey, F. M. Rodgers, R. D. Brown, Theory versus Experiment in Jet Spectroscopy: Glycolic Acid, *J. Am. Chem. Soc*., 1997, **119**, 2232–2239.

48 J. Thomas, N. A. Seifert, W. Jäger, Y. Xu, A Direct Link from the Gas to the Condensed Phase: A Rotational Spectroscopic Study of 2,2,2-Trifluoroethanol Trimers, *Angew. Chem. Int. Ed*., 2017, **56**, 6289 –6293.

49 S. Oswald, N. A. Seifert, F. Bohle, M. Gawrilow, S. Grimme, W. Jäger, Y. Xu, M. A. Suhm, The Chiral Trimer and a Metastable Chiral Dimer of Achiral Hexafluoroisopropanol: A Multi-Messenger Study, Angew. Chem. Int. Ed. 2019, 58, 5080 –5084

50 S. Ghosh, S. Bhattacharyya, S. Wategaonkar, Dissociation Energies of Sulfur Centered Hydrogen-Bonded Complexes, *J. Phys. Chem. A*, 2015, **119**, 10863−10870.

51 S. Bhattacharyya, S. Wategaonkar, ZEKE Photoelectron Spectroscopy of *p*-Fluorophenol···H_2S/H_2O Complexes and Dissociation Energy Measurement Using the Birge−Sponer Extrapolation Method, *J. Phys. Chem. A*, 2014, **118**, 9386−9396.

52 T. R. Dyke, K. M. Mack, J. S. Muenter, The Structure of Water Dimer from Molecular Beam Electric Resonance Spectroscopy, *J. Chem. Phys*., 1977, **66**, 498–510.

53 Q. Gou, L. Spada, M. Vallejo-López, A. Lesarri, E. J. Cocinero, W. Caminati, Interactions between alkanes and aromatic molecules: a rotational study of pyridine–methane, *Phys. Chem. Chem. Phys*., 2014, **16**, 13041–13046.

54 C. Pérez, I. León, A. Lesarri, B. H. Pate, R. Martínez, J. Millán, J. A. Fernández, Isomerism of the Aniline Trimer, *Angew. Chem. Int. Ed*., 2018, **57**, 15112–15116.

55 L. Goerigk, A. Hansen, C. Bauer, S. Ehrlich, A. Najibi, S. Grimme, A Look at the Density Functional Theory Zoo with the Advanced GMTKN55 Database for General Main Group Thermochemistry, Kinetics and Noncovalent Interactions, *Phys. Chem. Chem. Phys*., 2017, **19**, 32147–32744.

Scheme 1. Molecular formulas of the furfuryl alcohol (**1**) and furfuryl mercaptan (**2**) hydrates of ref. 25, compared with the thenyl mercaptan (**3**) and thenyl alcohol (**4**) water dimers.

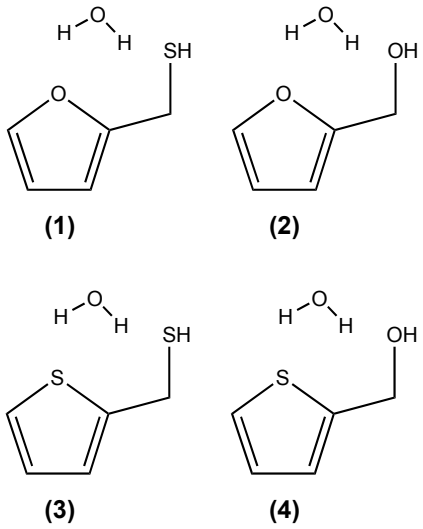

View Article Online
DOI: 10.1039/D0CP01706J

Figure 1. The microwave spectrum (2-8 GHz) of water-seeded thenyl alcohol, showing transitions from the TA monomer and the monohydrate TA···H_2O. The horizontal expansion (upper trace, 10 MHz) shows a typical torsional tunneling doubling in the rotational transition $2_{0,2}\leftarrow1_{0,1}$.

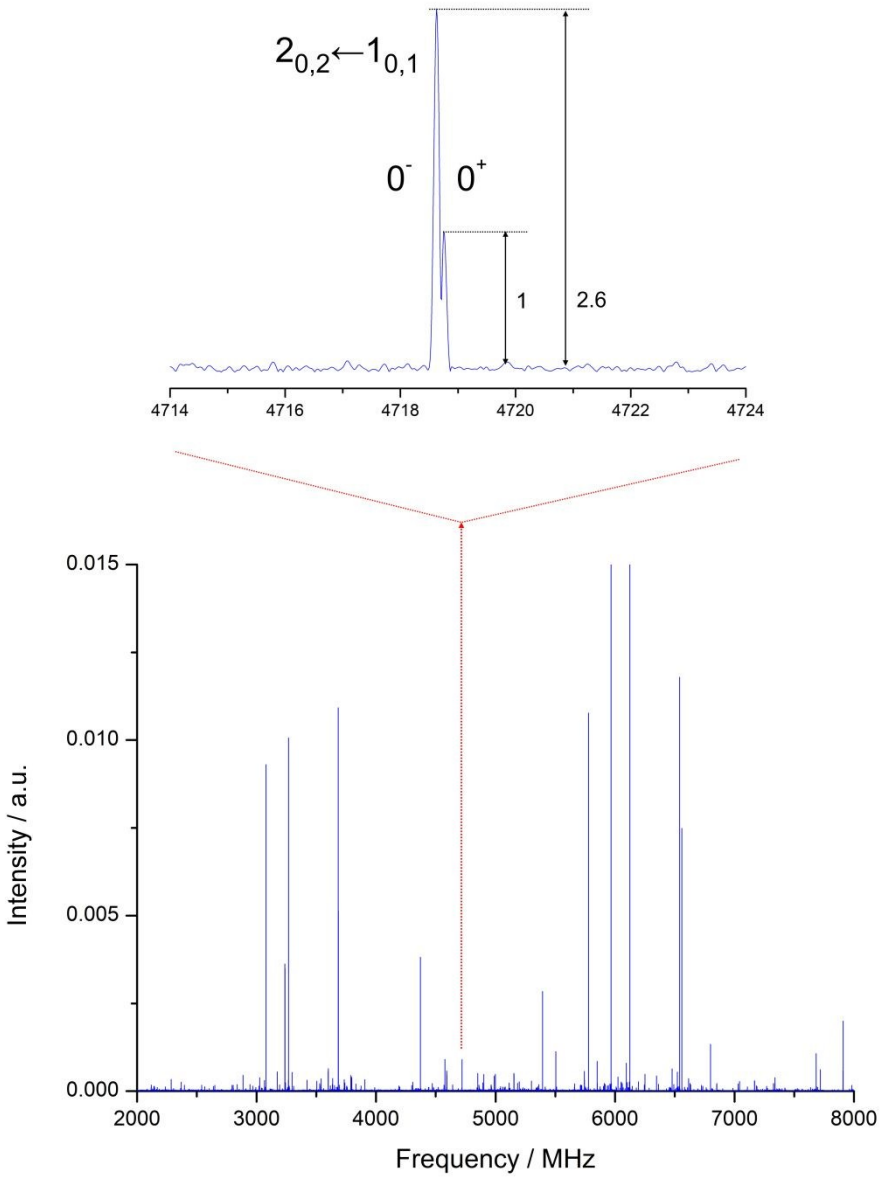

Figure 2. The microwave spectrum (2-8 GHz) of water seeded thenyl mercaptan showing transitions from the TM monomer and the monohydrate TM···H_2O. Torsional tunneling doublings in TM···H_2O are exemplified here for the transition $2_{1,2}\leftarrow1_{1,1}$.

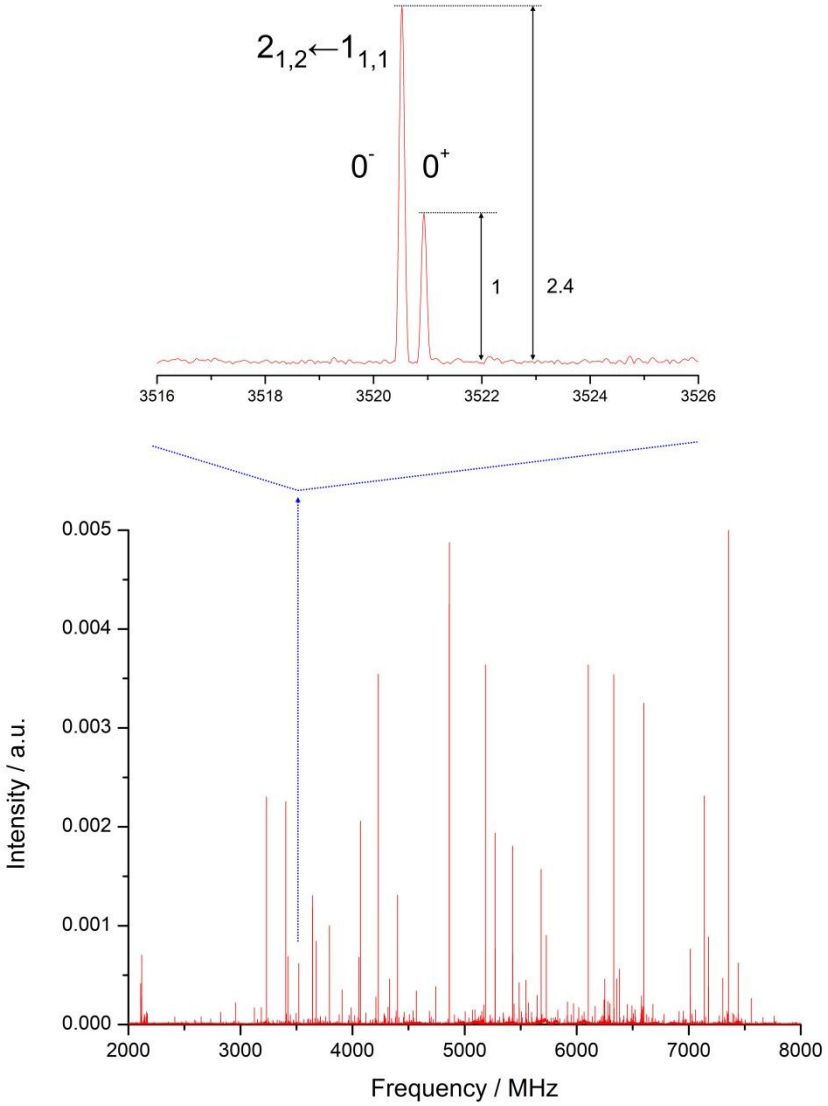

View Article Online
DOI: 10.1039/D0CP01706J

Figure 3. Conformational preferences for the thenyl alcohol monohydrate TA···H_2O with the experimentally observed isomer encircled. The Gibbs energies (kJ mol^{-1}) were predicted using B3LYP-D3(BJ) (red digits) or MN15-L (green digits) and the def2-TZVP basis set. The predicted H-bond distances are represented with a dotted line (B3LYP-D3(BJ)). The experimental value is represented in blue digits.

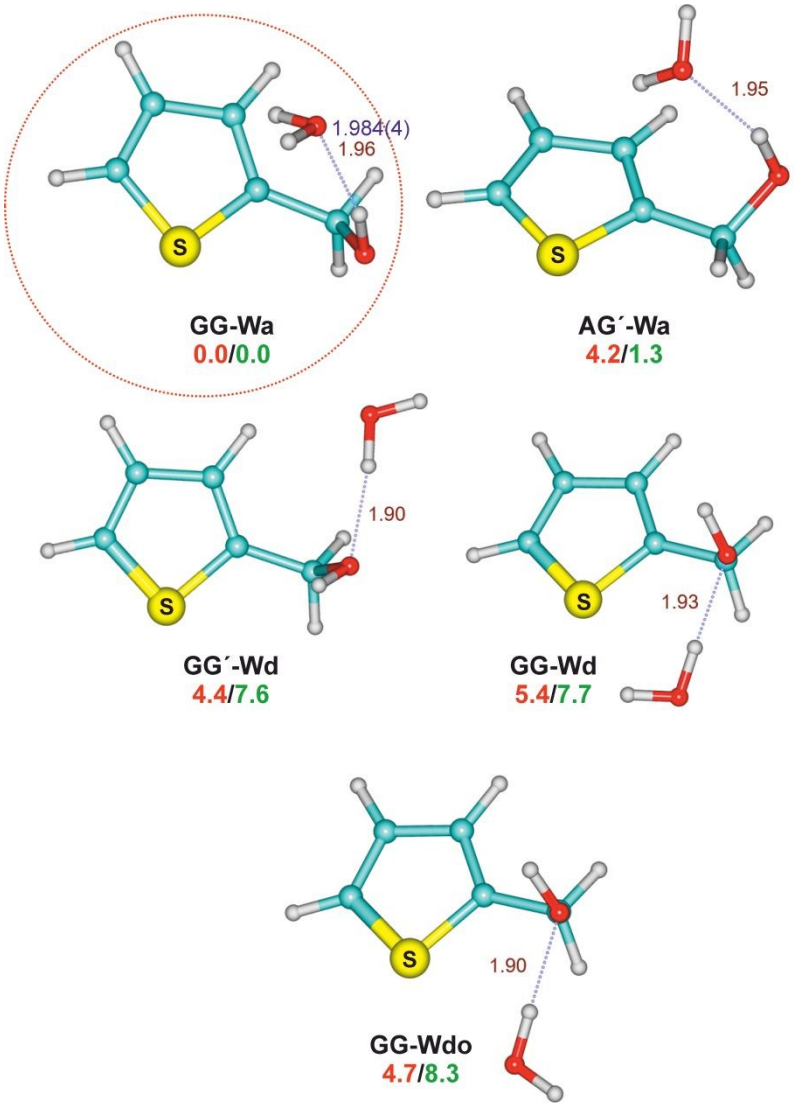

Figure 4. Conformational preferences for the thenyl mercaptan monohydrate TM···H_2O, showing the experimentally observed isomer (encircled) and the calculated Gibbs energies (kJ mol^{-1}, red digits: B3LYP-D3(BJ); green digits: MN15-L). The predicted H-bond distances are represented with a dotted line (B3LYP-D3(BJ)). The experimental value is represented in blue digits.

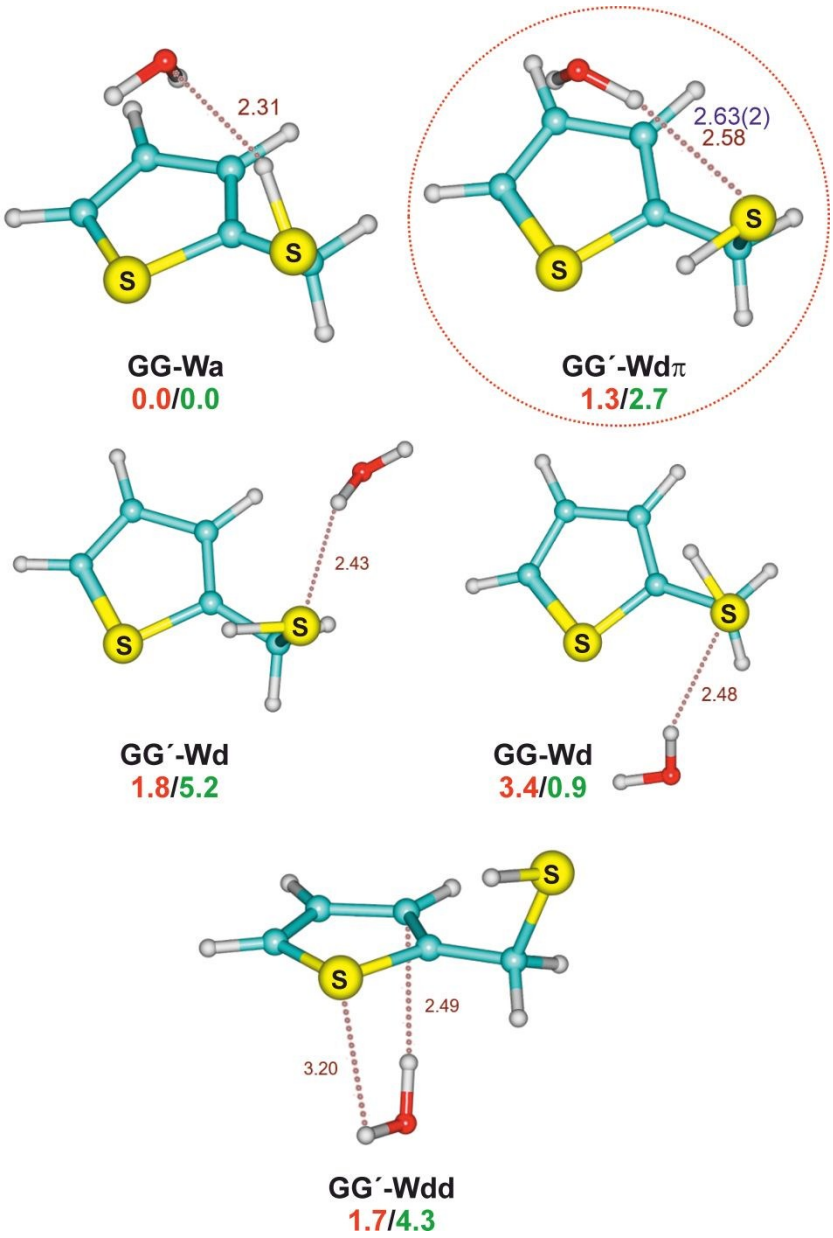

View Article Online
DOI: 10.1039/D0CP01706J

Figure 5. NCIPlot for the hydrates of thenyl alcohol and thenyl mercaptan (upper row) compared to furfuryl alcohol and furfuryl mercaptan (lower row), mapping noncovalent interactions. In this color scale blue shades indicate attractive interactions (associated to bond critical points), green colors indicate weak interactions and red represents repulsive interactions (like the ring critical points). See Fig. S3 (ESI†) for representations of the reduced electronic density in TA···H_2O and TM···H_2O. Oxygen and sulfur atoms are depicted conventionally in red and yellow, respectively.

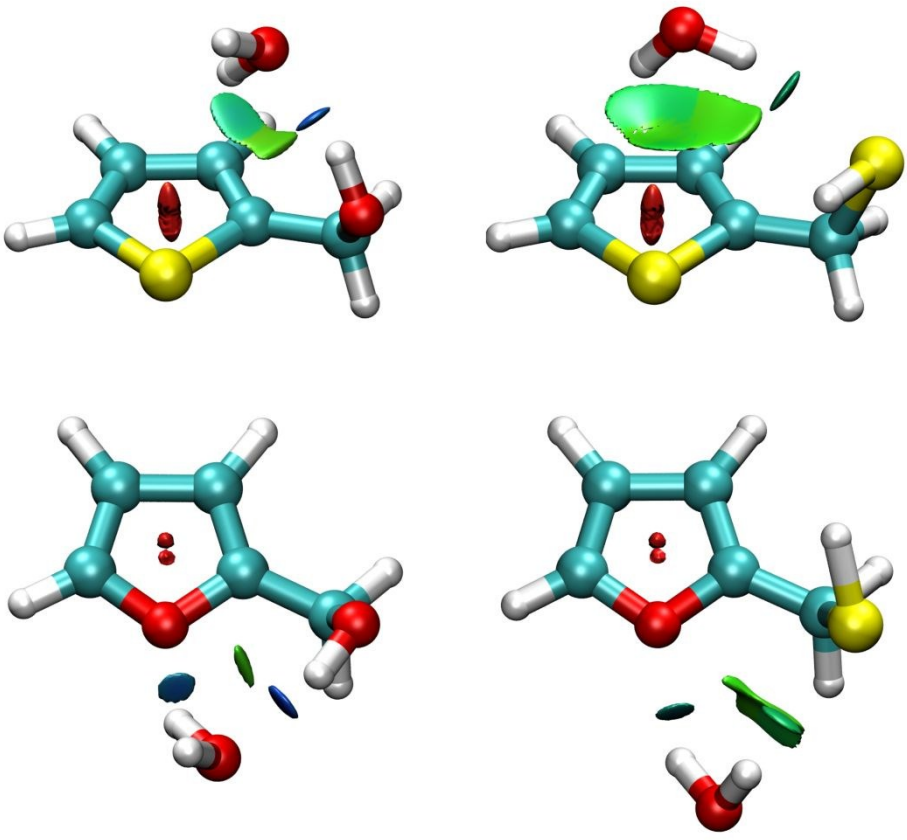

View Article Online
DOI: 10.1039/D0CP01706J

Table 1. DFT predictions for the thenyl alcohol monohydrate TA···H_2O.

	Isomer 1[c]	Isomer 2	Isomer 3	Isomer 4	Isomer 5
	GG-Wa	**AG´-Wa**	**GG´-Wd**	**GG-Wd**	**GG-Wdo**
A / MHz[a]	2227.45/2118.75	2326.07/2288.30	2762.34/2635.40	2737.55/2720.89	2797.43/2721.54
B / MHz	1276.12/1331.33	1177.28/1204.17	1060.18/1092.20	1144.32/1146.75	1121.00/1152.50
C / MHz	1110.86/1191.07	1050.38/1142.67	807.45/822.05	852.00/857.78	843.19/858.43
D_J / kHz	0.593/0.268	0.581/0.681	0.359/0.540	0.489/0.308	0.838/0.369
D_{JK} / kHz	1.875/ 1.112	1.165/0.988	-1.385/-2.570	-1.173/-0.408	-3.099/-0.655
D_K / kHz	-1.009/-0.160	0.161/0.483	4.856/7.246	4.803/2.277	7.307/2.647
d_1 / kHz	0.082/-0.022	0.045/-0.180	-0.102/-0.151	-0.159/-0.101	-0.280/-0.123
d_2 / kHz	-0.062/0.012	-0.053/-0.017	-0.007/-0.009	-0.015/-0.014	-0.020/-0.013
$\lvert\mu_a\rvert$ / D	2.59/2.74	1.62/1.69	0.64/0.44	3.65/3.17	1.19/0.90
$\lvert\mu_b\rvert$ / D	1.60/0.10	2.22/2.48	1.08/0.79	1.35/0.90	2.23/2.07
$\lvert\mu_c\rvert$ / D	0.19/0.62	0.02/0.29	0.34/0.55	1.43/1.49	0.30/0.45
ΔE /kJ mol^{-1}[b]	0.00/0.00	4.27/3.79	5.43/10.27	6.53/9.49	6.96/11.20
ΔG /kJ mol^{-1}	0.00/0.00	4.07/1.32	4.33/7.57	5.46/7.73	4.69/8.30
E_C / kJ mol^{-1}	-33.22/-34.56	-32.26/-34.39	-31.38/-28.83	-25.69/-24.89	-26.44/-23.77

[a]Rotational constants (A, B, C), Watson's S-reduction centrifugal distortion constants (D_J, D_{JK}, D_K, d_1, d_2) and electric dipole moments (μ_α, α = a, b, c). [b]Relative energies corrected with the zero-point energy (ZPE), Gibbs energy (ΔG, 298K, 1 atm) and complexation energy (including BSSE corrections). [c]B3LYP-D3(BJ) and MN15-L values, respectively (basis set def2TZVP)).

View Article Online
DOI: 10.1039/D0CP01706J

Table 2. DFT predictions for the thenyl mercaptan monohydrate TM···H_2O.

	Isomer 1[b]	**Isomer 2**	**Isomer 3**	**Isomer 4**	**Isomer 5**
	GG-Wa	**GG´-Wdπ**	**GG´-Wd**	**GG-Wd**	**GG-Wd**
A / MHz[a]	1942.58/1919.45	1885.74/1923.67	1991.10/1915.80	2029.86/2013.83	1874.66/1892.87
B / MHz	977.68/981.78	990.07/980.92	915.11/968.76	957.29/937.22	852.91/895.10
C / MHz	864.93/865.63	844.35/852.33	677.68/704.67	707.14/721.49	750.21/800.86
D_J / kHz	0.197/0.103	0.172/0.124	0.187/0.129	0.137/0.242	0.610/0.916
D_{JK} / kHz	1.735/0.962	1.343/0.855	0.0025/1.769	0.880/0.332	-0.760/15.231
D_K / kHz	-0.137/0.0545	0.037/0.250	1.889/-0.505	0.641/1.164	14.894/-14.319
d_1 / kHz	0.015/-0.004	0.0052/-0.006	-0.058/-0.033	-0.039/-0.037	-0.256/0.012
d_2 / *k*Hz	0.012/0.005	0.0010/0.004	-0.008/-0.030	-0.016/-0.069	-0.032/-0.048
$\lvert\mu_a\rvert$ / D	2.53/1.95	1.36/1.80	0.03/0.72	2.81/2.87	0.52/1.32
$\lvert\mu_b\rvert$ / D	1.09/2.15	3.03/2.31	0.28/0.63	1.12/0.67	2.06/1.24
$\lvert\mu_c\rvert$ / D	0.60/0.85	1.07/1.22	0.45/0.28	0.85/0.53	0.32/0.15
ΔE/ kJ mol^{-1}	0.00/0.00	0.06/2.66	1.99/6.93	3.37/5.95	7.14/11.17
ΔG /kJ mol^{-1}	0.00/0.00	1.27/2.65	1.79/5.22	3.38/0.90	1.68/4.33
E_C / kJ mol^{-1}	-23.10/-29.37	-24.14/-28.87	-25.44/-26.02	-21.00/-22.89	-15.36/-21.13

[a]Parameter definition as in Table 1. [b]B3LYP-D3(BJ) and MN15-L values, respectively (basis set def2TZVP)).

Table 3. Experimental rotational parameters for the thenyl alcohol monohydrate TA···H_2O.

	Isomer GG-Wa	
	0^-	0^+
A / MHz[a]	2194.4049(13)[c]	2194.4758(14)
B / MHz	1265.93407(41)	1265.93621(45)
C / MHz	1103.18208(23)	1103.23374(25)
D_J / kHz	0.7557(39)	
D_{JK} / kHz	1.987(37)	
D_K / kHz	-0.72(11)	
d_1 / kHz	0.0525(33)	
d_2 / kHz	-0.0414(36)	
$\lvert\mu_a\rvert$ / D	+ + +	+ + +
$\lvert\mu_b\rvert$ / D	+	+
$\lvert\mu_c\rvert$ / D		
N[b]	72	
σ / kHz	8.3	

[a]Rotational constants (A, B, C), Watson's S-reduction centrifugal distortion constants (D_J, D_{JK}, D_K, d_1, d_2) and electric dipole moments (μ_α, α = a, b, c). [b]Number of transitions (N) and rms deviation (σ) of the fit. [c]Standard errors in units of the last digit.

View Article Online
DOI: 10.1039/D0CP01706J

Table 4. Experimental rotational parameters for the thenyl mercaptan monohydrate TM···H_2O.

	Isomer GG′-Wdπ	
	0^-	0^+
A / MHz[a]	1861.917(13)	1862.71(10)
B / MHz	983.1121(10)	983.0283(30)
C / MHz	845.80995(49)	845.9741(24)
D_J / kHz	0.2403(55)	
D_{JK} / kHz	3.122(15)	
D_K / kHz	[0.]	
d_1 / kHz	0.0228(39)	
d_2 / kHz	[0.]	
$\lvert\mu_a\rvert$ / D	+ + +	+ + +
$\lvert\mu_b\rvert$ / D		
$\lvert\mu_c\rvert$ / D		
N	41	
σ / kHz	7.2	

[a]Parameter definition as in Table 3.

Table 5. Binding energy decomposition for the hydrates of tenyl alcohol (TA) and thenyl mercaptane (TM), and comparison with the hydrates of furfuryl alcohol (FA) and furfuryl mercaptan (FM), the dimers of H_2O and H_2S and the pyridine-methane dimer. The interaction energy is decomposed into electrostatic (ΔE_{elec}), inductive (multipole interactions/charge transfer, ΔE_{ind}), exchange repulsion (ΔE_{exch}) and dispersion (ΔE_{disp}) energy terms, using SAPT(0)/jun-cc-pVDZ (all values in kJ mol^{-1}). See Tables 1-2 for a comparison of complexation energies for TA···H_2O and TM···H_2O using DFT.

Cluster	ΔE_{elect}	ΔE_{disp}	ΔE_{ind}	ΔE_{exch}	ΔE_{total}
FA···H_2O (GG´-Wda)[a]	-61.3 [183.0%][f]	-14.6 [43.6%][f]	-17.7	60.1	-33.4
TA···H_2O (GG-Wa)[b]	-52.0 [179.9%]	-16.0 [55.4%]	-15.0	54.1	-28.9
$(H_2O)_2$[c]	-37.0 [169.7%]	-5.3 [24.3%]	-9.0	29.4	-21.8
FM···H_2O (GG´-Wda)[a]	-41.8 [196.2%]	-12.9 [60.6%]	-12.4	45.8	-21.3
FM···H_2O (GG-Wdd)[a]	-35.3 [171.4%]	-11.8 [57.3%]	-7.0	33.5	-20.6
Pyridine-methane[d]	-17.9 [100.6%]	-42.0 [236%]	-4.1	46.1	-17.8
TM···H_2O (GG´-Wdπ)[b]	-27.1 [154.4%]	-14.6 [83.3%]	-8.1	32.3	-17.6
$(H_2S)_2$[e]	-12.9 [286.7%]	-5.2 [115.6%]	-4.4	18.0	-4.5

[a]Ref. 25. [b]This work. [c]Ref. 52. [d]Ref. 53. [e]Ref. 11. [f]Percentage of the total binding energy.

View Article Online
DOI: 10.1039/D0CP01706J

TOC Graphic

Sulfur Hydrogen Bonding and Internal Dynamics in the Monohydrates of Thenyl Mercaptan and Thenyl Alcohol

M. Juanes, R. T. Saragi, R. Pinacho, J. E. Rubio, A. Lesarri,*

Water forms weak H-bonds with thenyl compounds, simultaneously retaining internal mobility in the dimer.